



HAL
open science

Reactivity of OH and CH₃OH between 22 and 64 K: Modelling the Gas Phase Production of CH₃O in Barnard 1B

M. Antiñolo, M. Agúndez, Elena Jimenez, B. Ballesteros, André Canosa,
Gisèle El Dib, J. Albaladejo, J. Cernicharo

► **To cite this version:**

M. Antiñolo, M. Agúndez, Elena Jimenez, B. Ballesteros, André Canosa, et al.. Reactivity of OH and CH₃OH between 22 and 64 K: Modelling the Gas Phase Production of CH₃O in Barnard 1B. *The Astrophysical Journal*, 2016, 823 (1), pp.25. 10.3847/0004-637X/823/1/25 . hal-01343402

HAL Id: hal-01343402

<https://univ-rennes.hal.science/hal-01343402>

Submitted on 12 Oct 2016

HAL is a multi-disciplinary open access archive for the deposit and dissemination of scientific research documents, whether they are published or not. The documents may come from teaching and research institutions in France or abroad, or from public or private research centers.

L'archive ouverte pluridisciplinaire **HAL**, est destinée au dépôt et à la diffusion de documents scientifiques de niveau recherche, publiés ou non, émanant des établissements d'enseignement et de recherche français ou étrangers, des laboratoires publics ou privés.



REACTIVITY OF OH AND CH₃OH BETWEEN 22 AND 64 K: MODELING THE GAS PHASE PRODUCTION OF CH₃O IN BARNARD 1b

M. ANTIÑOLO^{1,2}, M. AGÚNDEZ³, E. JIMÉNEZ^{1,2}, B. BALLESTEROS^{1,2}, A. CANOSA⁴, G. EL DIB⁴,
J. ALBALADEJO^{1,2}, AND J. CERNICHARO³

¹ Departamento de Química Física, Facultad de Ciencias y Tecnologías Químicas, Universidad de Castilla-La Mancha Avda. Camilo José Cela s/n, E-13071, Ciudad Real, Spain; elena.jimenez@uclm.es

² Instituto de Combustión y Contaminación, Universidad de Castilla-La Mancha. Camino de Moledores s/n, E-13071, Ciudad Real, Spain

³ Instituto de Ciencia de Materiales de Madrid, CSIC. C/ Sor Juana Inés de la Cruz 3, E-28049 Cantoblanco, Spain

⁴ Institut de Physique de Rennes, UMR 6251 CNRS-Université de Rennes 1, Campus de Beaulieu, Bât 11C, 263 Av. Général Leclerc, F-35042, Rennes, France; andre.canosa@univ-rennes1.fr

Received 2015 December 24; accepted 2016 March 13; published 2016 May 18

ABSTRACT

In recent years, ultra-low temperature chemical kinetic experiments have demonstrated that some gas-phase reactions are much faster than was previously thought. One example is the reaction between OH and CH₃OH, which has recently been found to be accelerated at low temperatures yielding CH₃O as its main product. This finding raised the question of whether or not the CH₃O observed in the dense core Barnard 1b could be formed by the gas-phase reaction of CH₃OH and OH. Several chemical models including this reaction and grain-surface processes have been developed to explain the observed abundance of CH₃O, but they have met with little success. Here, we report for the first time the rate coefficients for the gas-phase reaction of OH and CH₃OH down to a temperature of 22 K, which is very close to the temperature in cold interstellar clouds. Two independent experimental set-ups based on the supersonic gas expansion technique coupled to the pulsed laser photolysis laser-induced fluorescence technique were used to determine the rate coefficients in the temperature range 22–64 K. The temperature dependence obtained in this work can be expressed as $k(22\text{--}64\text{ K}) = (3.6 \pm 0.1) \times 10^{-12} (T/300\text{ K})^{-(1.0 \pm 0.2)} \text{ cm}^3 \text{ molecule}^{-1} \text{ s}^{-1}$. Implementing this expression in a chemical model of a cold, dense cloud results in CH₃O/CH₃OH abundance ratios similar to or slightly lower than the value of $\sim 3 \times 10^{-3}$ observed in Barnard 1b. This finding confirms that the gas-phase reaction between OH and CH₃OH is an important contributor to the formation of interstellar CH₃O. The role of grain-surface processes in the formation of CH₃O, although it cannot be fully neglected, remains controversial.

Key words: astrochemistry – ISM: molecules – molecular data – molecular processes

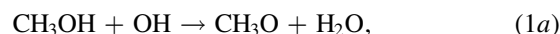
1. INTRODUCTION

Cold interstellar clouds are known to contain a rich variety of molecules whose synthesis has long been thought to rely on gas-phase ion–neutral chemical reactions (Herbst & Leung 1989). Since the 1990s, chemical kinetic experiments have demonstrated that many gas-phase neutral–neutral reactions in which at least one of the reactants is a radical are very rapid at low temperatures (Canosa et al. 2008; Smith & Barnes 2013), and thus play an important role in interstellar chemistry (Smith et al. 2004). Because cold interstellar clouds have extremely low temperatures, usually around 10 K, only gas-phase chemical reactions which are exothermic and barrierless are considered in the reaction networks currently used to model the chemistry of cold interstellar clouds (Agúndez & Wakelam 2013).

Recently, the reaction of hydroxyl (OH) radicals and methanol (CH₃OH) has experimentally been found to be very rapid at temperatures down to 56 K, despite the presence of an energy barrier, which is probably surpassed by quantum tunneling (Shannon et al. 2013; Gómez Martín et al. 2014). This finding has important potential implications for the chemistry of the interstellar medium. Indeed, the empirical evidence for a chemical reaction that overcomes an energy barrier at low temperatures opens the possibility of finding other reactions with similar behavior (see, e.g., Sims 2013) which could be potentially important for interstellar chemistry, although to date they are not included in chemical models. So

far, the reaction kinetic databases used to model interstellar chemistry, such as UMIST and KIDA (McElroy et al. 2013; Wakelam et al. 2015), have largely been based on data obtained at temperatures above 200 K (Atkinson et al. 2006). In particular, the rate constant of the reaction between OH and CH₃OH, which can be represented by the expression $2.85 \times 10^{-12} \exp(-345/T) \text{ cm}^3 \text{ molecule}^{-1} \text{ s}^{-1}$ in the temperature range 210–300 K (Atkinson et al. 2006), was previously presumed to be negligible at interstellar temperatures.

There are two possible pathways for the titled reaction:



The branching ratios of channels (1a) and (1b) were reported to depend on the temperature between 70 and 900 K (Shannon et al. 2013). At temperatures above 250 K, the formation of hydroxymethyl (CH₂OH) radicals is favored, while at much lower temperatures the formation of CH₃O via reaction (1a) was reported to be the major reaction pathway (Shannon et al. 2013). At 82 K, it was found experimentally that the formation of CH₃O in the reaction of OH with methanol occurs at a rate similar to that of the removal of OH radicals (Shannon et al. 2013). Master equation calculations performed by Shannon et al. (2013) corroborated the experimental observations and indicated that at 70 K, CH₃O radicals are expected to be formed with a >99%

yield. For that reason, channel (1a) and its rate coefficient, k_{1a} , are henceforth referred to as reaction (1) and k_1 , respectively. Cernicharo et al. (2012) recently detected CH₃O toward the cold, dense cloud Barnard 1b (B1-b) where the gas kinetic temperature is 10–15 K. Taking into account that methanol is ~ 300 times more abundant than CH₃O in B1-b (Öberg et al. 2010; Cernicharo et al. 2012), Cernicharo et al. suggested that the gas-phase reaction between OH and CH₃OH emerges as a potentially efficient way to form CH₃O in this source.

Soon after reaction (1) was empirically found to be accelerated at low temperatures with respect to room temperature (Shannon et al. 2013), the chemistry of cold dark clouds was revisited from a theoretical point of view (Vasyunin & Herbst 2013; Reboussin et al. 2014; Acharyya et al. 2015; Balucani et al. 2015; Kalvāns 2015; Ruaud et al. 2015). These studies were mainly dedicated to exploring the formation of complex organic molecules, such as CH₃OCH₃ and HCOOCH₃, although some of them also discussed the formation of CH₃O (Vasyunin & Herbst 2013; Acharyya et al. 2015; Balucani et al. 2015; Ruaud et al. 2015). The rate coefficient k_1 adopted by these authors was in agreement with the values reported by Shannon et al. (2013). The value of k_1 measured by Shannon et al. (2013) at 63 K was ca. $4 \times 10^{-11} \text{ cm}^3 \text{ molecule}^{-1} \text{ s}^{-1}$ and calculations performed by these authors indicate that by 20 K the rate coefficient has reached the collision limit ($3 \times 10^{-10} \text{ cm}^3 \text{ molecule}^{-1} \text{ s}^{-1}$). Extending the temperature range down to 56 K, Gómez Martín et al. (2014) measured a rate coefficient of ca. $5 \times 10^{-11} \text{ cm}^3 \text{ molecule}^{-1} \text{ s}^{-1}$ and, using their kinetic data in the range 56–88 K, reported an extrapolated value of k_1 at 0 K of ca. $6 \times 10^{-11} \text{ cm}^3 \text{ molecule}^{-1} \text{ s}^{-1}$, which suggests a less pronounced increase of k_1 with decreasing temperature than predicted by Shannon et al. (2013). The value of k_1 adopted by chemical models of cold, dark clouds that have addressed the formation of CH₃O has been either $4 \times 10^{-11} \text{ cm}^3 \text{ molecule}^{-1} \text{ s}^{-1}$ or $3 \times 10^{-10} \text{ cm}^3 \text{ molecule}^{-1} \text{ s}^{-1}$.

In this paper, we present the first determination of the rate coefficients for the reaction of OH with CH₃OH at temperatures down to 22 K, which allows us to obtain the first complete picture of the temperature dependence of k_1 at temperatures below 50 K and much closer to the typical temperatures, ~ 10 K, found in dark molecular clouds. In light of the new rate coefficients reported here, we also re-evaluate whether the gas-phase route involving reaction (1a) is able by itself to explain the CH₃O abundance observed in B1-b. For this purpose, we model the chemistry of cold dense clouds, adopting the extrapolated value of k_1 at 10 K from the temperature dependence observed in this work.

2. METHODS

2.1. Measurement of the Rate Coefficients for Reaction (1) at Ultra-low Temperatures

2.1.1. Ultra-cold Environment: Uniform Supersonic Gas Expansion Technique

The CRESU (*Cinétique de Réaction en Ecoulement Supersonique Uniforme*, which means Reaction Kinetics in a Uniform Supersonic Flow) technique has been used in this work to cover the temperature range 22–64 K. Two independent apparatus were employed. These are the CRESU apparatus recently constructed at the University of Castilla-La

Table 1

Summary of the Experimental Conditions in the Employed CRESU Systems

Bath Gas	P_{res} (mbar)	P_{cham} (mbar)	M	T (K)	CRESU System
He	337.0	0.621	6.1 ± 0.2	22.4 ± 1.4	UCLM ^a
N ₂ /He	127.1	0.296	5.0 ± 0.1	42.5 ± 1.3	UCLM ^b
N ₂	107.3	0.180	5.09 ± 0.04	47.7 ± 0.6	UR1 ^c
N ₂	136.2	0.279	4.9 ± 0.1	51.6 ± 1.7	UCLM ^b
Ar	28.20	0.390	3.73 ± 0.04	52.2 ± 0.9	UR1 ^c
N ₂	41.75	0.184	4.36 ± 0.05	61.0 ± 1.0	UR1 ^c
N ₂	41.67	0.183	4.2 ± 0.1	64.2 ± 1.7	UCLM ^b

Notes. P_{res} is the pressure in the reservoir, P_{cham} the pressure in the chamber, M the Mach number, and T the temperature of the jet. Uncertainties are $\pm 1\sigma$ and reflect aerodynamic fluctuations along the supersonic flow axis.

^a Pulsed mode (see more details in Jiménez et al. 2015).

^b Continuous mode (see Jiménez et al. 2016).

^c Sims et al. (1994), Canosa et al. (2008).

Mancha (hereafter referred as the UCLM system) and the CRESU system available at the University of Rennes 1 (hereafter referred as UR1 system). UCLM CRESU was used to investigate the kinetics of OH and methanol at four temperatures (22, 42, 52, and 64 K), whereas the UR1 CRESU system operated at three temperatures (48, 52, and 61 K).

As both systems have previously been described elsewhere (Sims et al. 1994; Canosa et al. 2008; Jiménez et al. 2015, 2016), only some remarks are mentioned here. In both CRESU systems, a stainless steel chamber is connected to a pumping system to generate low pressures inside (P_{cham}). A supersonic flow is achieved by the isentropic expansion of a buffer gas through a specifically designed Laval nozzle separating a movable stagnation reservoir maintained at room temperature from the main vacuum chamber. The quality and physical conditions of the flow directly depend on the geometry of the Laval nozzle on the one hand, and on the nature and flow rate of the buffer gas on the other hand. The gas flows through the reservoir at a constant flow rate, providing a constant background pressure P_{cham} , when using a suitable pumping speed. The UCLM system can operate with a gas flow in either pulsed or continuous mode, while the UR1 system is operating exclusively in the latter mode. In the UCLM pulsed mode ($T = 22$ K), the movable expansion system also included a rotary disk (aerodynamic chopper) in order to pulse the gas inside the Laval nozzle, while in the continuous mode ($T = 42, 52, 64$ K) the gas is constantly flowing through one of the apertures of the aerodynamic chopper maintained at rest. In the UR1 system, there is no rotary disk in the movable expansion system. In Table 1, a summary of the experimental conditions is presented for both CRESU systems. In the UCLM system, the same convergent–divergent Laval nozzle was operated under different physical conditions to achieve the desired temperatures and gas densities. For temperatures higher than 22 K, the bath gas, helium, was changed by nitrogen or a mixture of both gases, as previously described in Jiménez et al. (2016). In the UR1 system, nitrogen or argon was used as a bath gas to obtain the three different temperature conditions, each of which were achieved using a different Laval nozzle.

2.1.2. Kinetic Technique and Determination of the Rate Coefficients k_1

To carry out the kinetic experiment of reaction (1), the OH radicals first have to be generated in situ. In this work, the

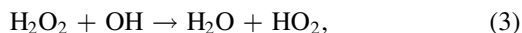
Pulsed Laser Photolysis (PLP) of gaseous H_2O_2 ,



was the source of OH radicals in both CRESU systems.

The photolysis wavelengths were 248 nm (from a KrF excimer laser in UCLM) and 266 nm (from the fourth harmonic of a Nd-YAG laser in UR1). Laser energies, measured at the laser exit and at 10 Hz, were 10 and 75 mJ per pulse, respectively. Gaseous H_2O_2 was introduced into the reservoir by passing a small flow of the bath gas through a concentrated solution of H_2O_2 contained in a glass bubbler. An aqueous solution of H_2O_2 , which was provided by Sharlab at a concentration of 50% v/v, was further purified by bubbling helium or nitrogen through the liquid for a few days in order to remove water at least partly. Concentrations of about 70% were obtained with this method for the H_2O_2 in the solution. Liquid samples of methanol (with a purity $\geq 99.8\%$ in UCLM and HPLC grade in UR1) were degassed prior to its use. The introduction of methanol in the reservoir was made differently in UCLM and in UR1. In the UCLM system, mixtures of methanol vapour and the bath gas were prepared and stored in two 20 L glass bulbs prior to the experiments. Then, the content of the storage bulbs was directed into the reservoir by means of a calibrated mass flow controller. In the UR1 set-up, gaseous methanol was introduced into the reservoir in a manner similar to H_2O_2 , i.e., by passing a bath gas identical to the main buffer gas through a bubbler containing liquid CH_3OH . The temperature and pressure were measured in the bubbler during the experiments. The partial flow of methanol was then obtained knowing the bath gas flow rate as well as the vapour pressure of CH_3OH at the bubbler temperature (see El Dib et al. 2013 for details). In both CRESU systems, a third flow of the buffer gas was introduced into the reservoir through a separate entry port to reach the desired reservoir pressure P_{res} . This flow is the main contributor to the total gas flow through the reservoir.

In the presence of an excess of methanol, i.e., under pseudo-first-order conditions where $[\text{CH}_3\text{OH}] \gg [\text{OH}]$ and $[\text{H}_2\text{O}_2] \gg [\text{OH}]$, the reaction scheme is described by reaction (1), the reaction of OH with H_2O_2 (reaction (3)), and other losses of OH, such as diffusion or reaction with impurities, if any (reaction (4)):



Under our experimental conditions, reaction (4) can be neglected since, in the absence of methanol, the loss of OH radicals is governed by reaction with H_2O_2 , which is in large excess.

To obtain the kinetic information, the OH radicals formed in reaction (2) are excited at 282 nm (radiation from a frequency-doubled dye laser pumped either by a XeCl excimer laser in UCLM or a 532 nm Nd-YAG laser in UR1). The laser-induced fluorescence (LIF) from excited OH radicals was detected at ca. 310 nm by a photomultiplier tube as a function of reaction time. The timescale of the reaction, which depends on the rate coefficient k_1 and the concentration of methanol introduced into the reservoir, must be short enough to be smaller than or of the same order of magnitude as the hydrodynamic time during which the supersonic flow is kept uniform (usually several hundreds of μs , with the exact value being specific to each flow condition validated for a given Laval nozzle). At short reaction

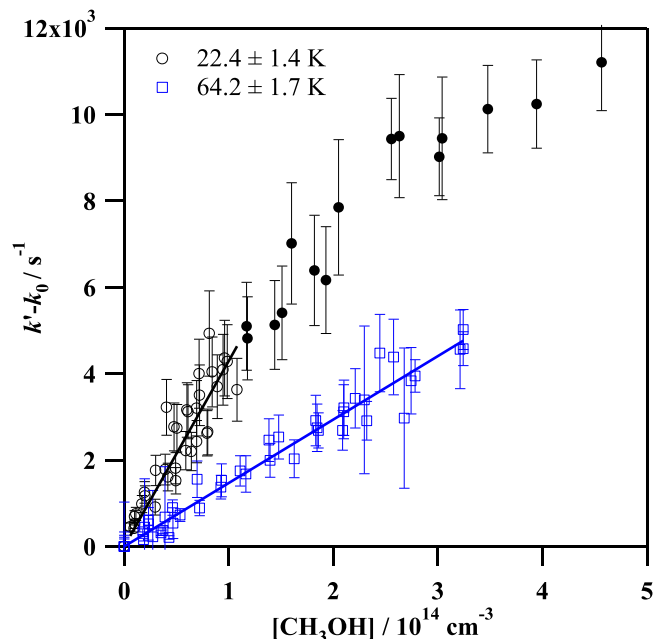


Figure 1. Plot of $k' - k_0$ vs. $[\text{CH}_3\text{OH}]$ at 22 and 64 K. Full black circles, which correspond to kinetic data at 22 K that are influenced by methanol clustering ($[\text{CH}_3\text{OH}] > 1 \times 10^{14}$ molecule cm^{-3} , see text), have not been considered in the fit of Equation (5).

times (tens of μs), the LIF signal from excited OH increases due to rotational relaxation, and so in the analysis of the OH temporal profiles, only the decay of the LIF signal at $t > 20 \mu\text{s}$ is considered. The analysis of the exponential decays yields the pseudo-first-order rate coefficients, k' , which are linearly related to $[\text{CH}_3\text{OH}]$ under pseudo-first-order conditions:

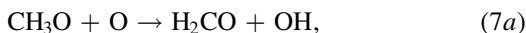
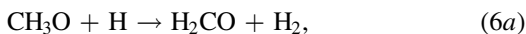
$$k' = k_0 + k_1(T)[\text{CH}_3\text{OH}], \quad (5)$$

where $k_1(T)$ is the bimolecular rate coefficient for reaction (1) at a given temperature and k_0 is the measured rate coefficient in the absence of methanol at the same temperature when only reactions (3) and (4) take place. k_0 ranged between 2800 and 8400 s^{-1} . This meant that the contribution of k_0 to k' was very variable, between 40% and 95%, although it typically did not exceed 70%. By varying the concentration of methanol and maintaining as constant the concentration of the precursor of OH radicals, $k_1(T)$ can be obtained from the slope of the plot of k' (or $k' - k_0$) versus $[\text{CH}_3\text{OH}]$. In the present study, we have chosen the second option because it is the only way to compare results obtained at the same temperature in independent experiments, in which k_0 may differ up to 2000 s^{-1} . Methanol concentrations were varied in UR1 by changing the pressure inside the CH_3OH bubbling column using a micrometric valve. In UCLM, $[\text{CH}_3\text{OH}]$ was varied by changing the mass flow rate of the diluted mixture from the storage bulb. Examples of plots of $k' - k_0$ versus $[\text{CH}_3\text{OH}]$ are presented in Figure 1. In the UCLM system, up to 48 kinetic experiments were carried out at a single temperature, using different mixing ratios of the CH_3OH /bath gas mixtures in the storage bulb. In the UR1 apparatus, between 14 and 21 kinetic experiments were performed for each Laval nozzle.

2.2. Chemical Model

In order to evaluate the role of reaction (1) in the formation of CH₃O in B1-b, we built a chemical model adopting typical conditions of a cold dense cloud, i.e., a temperature of 10 K, a visual extinction of 30 mag, a cosmic-ray ionization rate of H₂ of $1.3 \times 10^{-17} \text{ s}^{-1}$, and so-called “low-metal” elemental abundances (see Agúndez & Wakelam 2013). According to Daniel et al. (2013), the volume density of H₂ in B1-b has a steep radial gradient and takes values from a few 10^6 cm^{-3} at the core center to $\sim 10^4 \text{ cm}^{-3}$ in the outer regions of the cloud (at some tens of arcsec from the center). Since methanol has a widespread distribution in B1-b (Öberg et al. 2010) and methoxy probably has a similar distribution, we adopted densities of H nuclei of $2 \times 10^4 \text{ cm}^{-3}$ and $1 \times 10^5 \text{ cm}^{-3}$ to investigate the effect of density. Since grain-surface chemistry is hampered by the low mobility of most species on ice surfaces at the low temperatures of dust in cold, dense clouds, and since we aim to evaluate the efficiency of gas-phase routes to CH₃O, we did not consider chemical reactions on grain surfaces other than the formation of H₂ by the recombination of two H atoms. We adopted the gas-phase reaction network of Ruaud et al. (2015) with the rate coefficient for reaction (1) updated according to this work. Since it is well known that pure gas-phase chemical models severely underestimate the gas-phase abundance of CH₃OH in cold dense clouds (e.g., Agúndez & Wakelam 2013), to be more realistic, we assumed an abundance of methanol relative to CO of 6×10^{-5} , which is the value in B1-b according to the abundances of CO and CH₃OH derived by Lis et al. (2002) and Öberg et al. (2010), respectively.

The kinetic information on the gas-phase reactivity of CH₃O is quite scarce and is limited to temperatures above 200 K. Theoretical and experimental studies indicate that reactions of CH₃O with molecules such as H₂, CO, CH₄, NH₃, or CH₃OH have important activation barriers (Sanders et al. 1980; Jodkowski et al. 1999; Wang et al. 1999). The depletion of CH₃O in cold, dense clouds is likely to be dominated by reactions with H and O atoms,



whose rate coefficients are, however, not known at interstellar temperatures. We have adopted the same values used by Ruaud et al. (2015)⁵ for $k_{6a,b}$ and $k_{7a,b}$, which are based on measurements at 300 K (Hoyermann et al. 1981; Ewig et al. 1987; Dóbbé et al. 1991; Baulch et al. 2005). Therefore, in the absence of grain-surface processes, the chemistry of CH₃O becomes rather simple in the model as it is assumed to be formed through reaction (1) and destroyed by reactions (6) and (7). Therefore, at steady state, the CH₃O/CH₃OH abundance ratio is given by

$$\frac{[\text{CH}_3\text{O}]}{[\text{CH}_3\text{OH}]} = \frac{k_1[\text{OH}]}{k_6[\text{H}] + k_7[\text{O}]}, \quad (8)$$

⁵ Note that the rate coefficient of reaction (7b) given in Table A2 of Ruaud et al. (2015) should read $1.9 \times 10^{-11} \text{ cm}^3 \text{ molecule}^{-1} \text{ s}^{-1}$ instead of $1.9 \times 10^{-12} \text{ cm}^3 \text{ molecule}^{-1} \text{ s}^{-1}$.

Table 2
Gas-phase Rate Coefficients of the Reaction between OH
and CH₃OH Determined in This Work

T (K)	n (10^{16} cm^{-3})	k_1 ($10^{-11} \text{ cm}^3 \text{ molecule}^{-1} \text{ s}^{-1}$)
22.4 ± 1.4	17.0 ± 1.6	4.30 ± 0.66
42.5 ± 1.3	5.22 ± 0.33	2.74 ± 0.42
47.7 ± 0.6	2.74 ± 0.09	2.17 ± 0.35
51.6 ± 1.7	4.17 ± 0.35	2.19 ± 0.26
52.2 ± 0.9	5.15 ± 0.13	2.97 ± 0.60
61.0 ± 1.0	2.02 ± 0.08	2.11 ± 0.75
64.2 ± 1.7	2.24 ± 0.15	1.47 ± 0.23

Note. Uncertainties in the rate coefficient measurements are the combination of statistical errors ($\pm 1\sigma$, Student t factor at 95% confidence level) and systematic errors (15%). Uncertainties given for T and n are $\pm 1\sigma$.

where k_1 is well constrained by our experiments, and thus the major source of uncertainty in the calculated CH₃O/CH₃OH abundance ratio comes from the values of k_6 and k_7 at low temperatures.

3. RESULTS AND DISCUSSION

3.1. Evaluation of the Role of Secondary Chemistry of Methanol in the Determination of $k_1(T)$

Knowledge of the methanol concentration is one of the key parameters for deriving a reliable rate coefficient from Equation (5). For that reason, an evaluation of the potential effect of any side reaction that could deplete methanol is desirable.

No photolysis of methanol is expected at the photolysis (248 or 266 nm) and excitation (282 nm) wavelengths at the concentration levels and the low laser fluences (i.e., less than 1 mJ cm^{-2} per laser pulse measured at the exit of the nozzle in UCLM) used in this work, if we consider an upper limit for the absorption cross-section of $10^{-22} \text{ cm}^2 \text{ molecule}^{-1}$ (Cheng et al. 2002).

As can be seen in Figure 1, a slight curvature in the plots of $k' - k_0$ versus [CH₃OH] was observed at methanol concentrations higher than $1 \times 10^{14} \text{ molecule cm}^{-3}$ for the lowest temperature, 22 K. This curvature was also observed by Gómez Martín et al. (2014) at 56 K for reaction (1) for methanol concentrations higher than $2.5 \times 10^{14} \text{ molecule cm}^{-3}$. This may be explained by a clustering process that reduces the amount of methanol available for reacting with OH radicals, leading to a decrease of the measured pseudo-first-order rate coefficient k' . The lower the temperature is, the more favorable the cluster formation is, shifting the curvature in the pseudo-first-order plots to much lower methanol concentrations. Laksmono et al. (2011) observed the formation of clusters of methanol, and even the formation of small droplets in the divergent section of a Laval nozzle at 210 K, although the methanol concentration in their experiments was around 4 orders of magnitude higher than in ours. Therefore, we believe that under our experimental conditions the clusters that are formed are mainly methanol dimers. In order to estimate the effect of dimerization in the measurement of the pseudo-first-order coefficients, a simple model has been developed using FACSIMILE software for the worst scenario, i.e., the lowest temperature where the gas density is the highest (see Table 2). The reaction scheme of this model includes reactions (1) and

(3), together with the formation of a hydrogen-bonded methanol dimer:



In the simulation, $k_1(T)$ and the pseudo-first-order k' in the absence of methanol were fixed to the value obtained from the linear fit according to Equation (5) and the experimental k_0 . It was also considered that the dimer does not react with OH radicals. We estimate that the observed curvature is compatible with a rate coefficient for the dimerization of methanol at 22 K of the order of $10^{-11} \text{ cm}^3 \text{ molecule}^{-1} \text{ s}^{-1}$. The effect of dimerization on k' can be neglected at concentrations lower than $1 \times 10^{14} \text{ molecule cm}^{-3}$, i.e., those considered in this study. For intermediate temperatures, the concentration range was also constrained to $[\text{CH}_3\text{OH}]$ below $2 \times 10^{14} \text{ molecule cm}^{-3}$, while at 64 K the maximum methanol concentration was kept below $3.5 \times 10^{14} \text{ molecule cm}^{-3}$. Consequently, only the linear part of these plots was considered in obtaining $k_1(T)$.

3.2. Potential Role of Water in the Determination of $k_1(T)$

Water, which was introduced in conjunction with H_2O_2 into the reactor, did not play any significant role in the chemistry of the flow. Its potential aggregation to methanol to form a $\text{H}_2\text{O} \cdots \text{CH}_3\text{OH}$ complex was found to be a negligible process in the loss of methanol. Indeed, water concentration in the cold flow was estimated to be similar to that of H_2O_2 taking into account the concentration ratios in the liquid mixture and the vapor pressures of H_2O and H_2O_2 , 42.4 mbar and 24.4 mbar at 300 K, respectively. The H_2O_2 concentration was evaluated using a room temperature UV absorption column set in between the H_2O_2 bubbler and the reservoir at the pressure condition of our experiment at 64 K. The obtained concentration converted into the supersonic flow conditions was found to be about $6 \times 10^{12} \text{ cm}^{-3}$, representing a few percent of the typical $[\text{CH}_3\text{OH}]$ used in this experiment (see Figure 1). The work of Vöhringer-Martínez et al. (2007) on the catalytic effect of water on the OH + acetaldehyde gas-phase reaction between 58 and 300 K indicates that at temperatures below 100 K, the complexation of acetaldehyde molecules with water is highly efficient, although at high water concentrations (3% of the total density, i.e., $2.55 \times 10^{15} \text{ cm}^{-3}$ at 77 K). In the work of Vöhringer-Martínez et al. (2007), the $[\text{H}_2\text{O}]/[\text{CH}_3\text{CHO}]$ ratio is around 16. In our work, at 64 K, $[\text{H}_2\text{O}]$ in the supersonic jet is estimated to be on the order of 10^{13} cm^{-3} , and therefore the $[\text{H}_2\text{O}]/[\text{CH}_3\text{OH}]$ ratio is <0.1 . Water content accounts for 0.04% of the total gas density ($2.24 \times 10^{16} \text{ cm}^{-3}$), i.e., it is negligible. Moreover, Vöhringer-Martínez et al. (2007) concluded that at water contents lower than 3%, no catalytic effect was observed for the OH+acetaldehyde system. Under our experimental conditions, if a $\text{H}_2\text{O} \cdots \text{CH}_3\text{OH}$ cluster is formed with an aggregation factor of unity (as suggested by Vöhringer-Martínez et al. 2007 at $T < 100 \text{ K}$), and assuming that the kinetics of the dimer formation is fast enough to produce it in the timescale of our experiment (300 microseconds), then the methanol concentration would only be slightly reduced, and thus would not affect the measured rate coefficient.

3.3. Rate Coefficients $k_1(T)$ between 22 and 64 K

In light of the absence of any secondary chemistry under our experimental conditions, $k_1(T)$ were obtained as described in

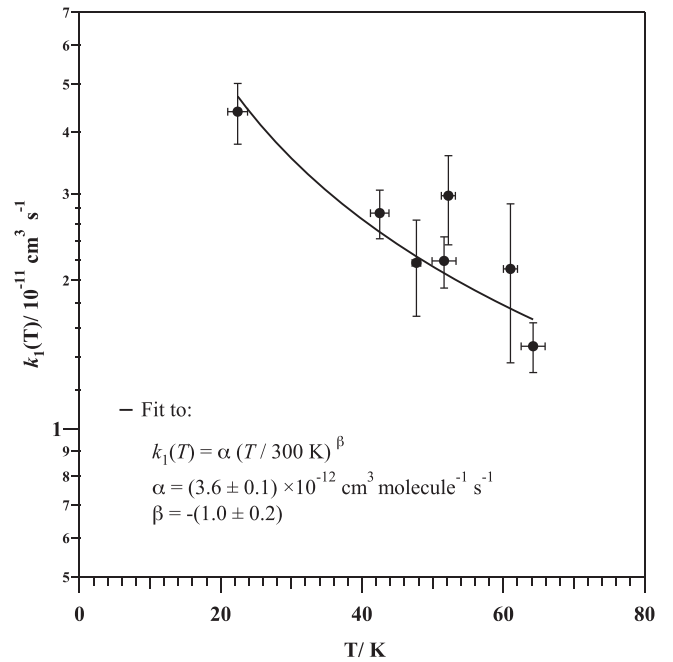


Figure 2. Rate coefficients for the reaction of OH with CH_3OH as a function of temperature determined in this work between 22 and 64 K. The black line corresponds to Equation (10).

Section 2 and are shown in Table 2. Statistical errors in $k_1(T)$ result from a least-squares analysis of the pseudo-first-order rate coefficient multiplied by the Student t factor corresponding to the 95% confidence limit. The errors given in Table 2 also include the contribution from systematic errors, estimated to be about 15%, which essentially come from uncertainties in mass flows or pressure gauge calibrations, and fluctuations in the temperature and concentration of methanol. The total gas densities are also listed in Table 2. Note that the study of any pressure dependence of the rate coefficient is not possible for a single Laval nozzle operating with a specific bath gas and at a fixed temperature. Nevertheless, no pressure dependence of $k_1(T)$ seems to exist at ultra-low temperatures, according to Shannon et al. (2013), and so the results obtained for the temperatures employed in this work at different gas densities can be compared.

The rate coefficients $k_1(T)$ obtained in this work between 22 and 64 K are depicted in Figure 2 in a semi-log form. It can be seen that $k_1(T)$ increases as the temperature decreases, i.e., it shows a negative temperature dependence. The data points have been fit in the temperature range 22–64 K to the expression

$$k_1(T) = (3.6 \pm 0.1) \times 10^{-12} \left(\frac{T}{300 \text{ K}} \right)^{-(1.0 \pm 0.2)}, \quad (10)$$

where $k_1(T)$ has units of $\text{cm}^3 \text{ molecule}^{-1} \text{ s}^{-1}$. The extrapolation of Equation (10) to a temperature of 10 K, which is of interest for cold, dark clouds such as B1-b, yields a value of $1.1 \times 10^{-10} \text{ cm}^3 \text{ molecule}^{-1} \text{ s}^{-1}$. It is worth noting that for the present limited experimental temperature range, several mathematical expressions give fairly acceptable fits. However, for some of these expressions, the extrapolation beyond the experimental temperature range, especially at temperatures significantly below 22 K, can diverge or result in unrealistic

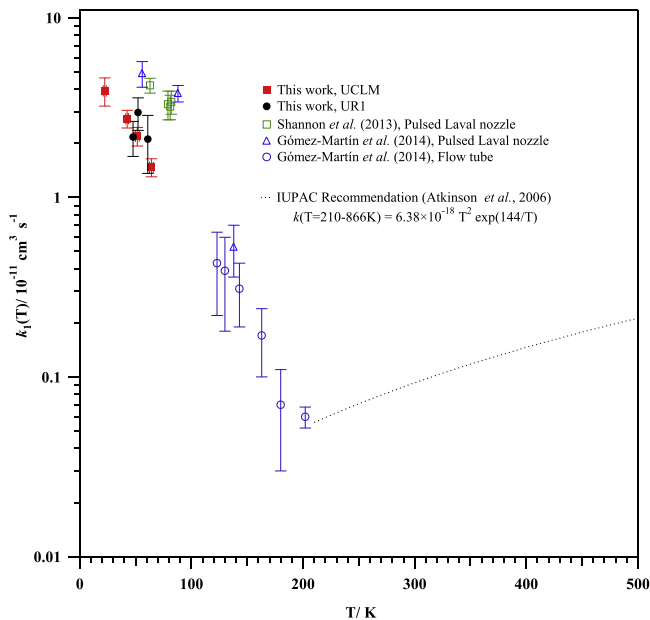


Figure 3. Rate coefficients for the reaction of OH with CH₃OH as a function of temperature. Filled symbols are kinetic data presented in this work and empty symbols are values reported in the literature.

rate coefficients. Future works, which require the construction of new Laval nozzles, are planned to extend the present temperature range in order to better constrain the dependence with temperature k_1 .

For comparison purposes, values of k_1 reported at temperatures higher than 56 K are depicted in Figure 3. The methanol reactivity toward OH radicals at 22 K is enhanced by almost two orders of magnitude compared to 200 K (Gómez Martín et al. 2014). The negative temperature dependence of $k_1(T)$ was already observed by Shannon et al. (2013) and Gómez Martín et al. (2014) in the 56–202 K range. Nevertheless, the values of $k_1(T)$ previously determined by these authors using a pulsed Laval nozzle are around twice as high as ours in the temperature range common to these authors and as well as our work (close to 60 K). The source of this discrepancy is presently unknown and deserves more experimental attention. The good agreement observed in the present study employing two independent CRESU machines provides confidence to the values reported here. Furthermore, the trend observed in this work between 22 and 64 K is consistent with the results obtained by Gómez Martín et al. (2014) between 123 and 202 K using a classical flow tube coupled to a PLP-LIF technique.

At temperatures between 210 and 866 K, the trend in the temperature dependence of $k_1(T)$ is inverted, showing a positive temperature dependence (Atkinson et al. 2006). This opposite behavior yields a “U shape” in the $\log k_1(T)$ versus T plots, which has already been observed for other reactions of OH with complex organic molecules (Shannon et al. 2010, 2014; Caravan et al. 2015; Jiménez et al. 2015, 2016). At ultra-low temperatures, the reaction mechanism that allows this to occur is one in which an adduct is formed by a weak hydrogen-bonded association of OH and methanol followed by quantum-mechanical tunneling, as suggested by Shannon et al. (2013). Recently, Hernandez et al. (2015) reported experimental evidence for the formation of hydrogen-bonded intermediate OH...CH₃OH by He Nanodroplet Isolation (HENDI) and a

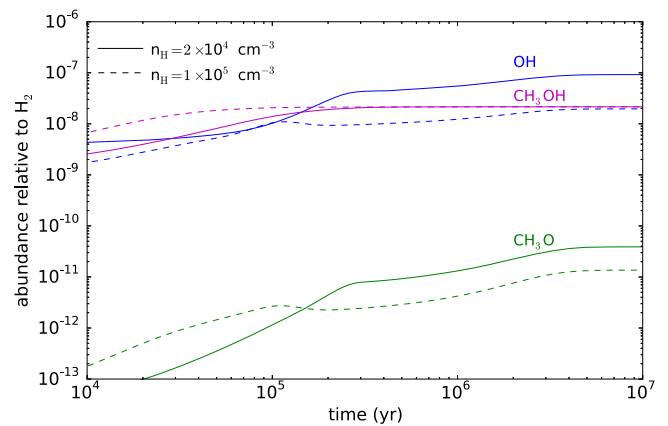


Figure 4. Calculated abundances of OH, methanol, and CH₃O relative to H₂ are shown as a function of time. Solid and dashed lines correspond to densities of H nuclei of $2 \times 10^4 \text{ cm}^{-3}$ and $1 \times 10^5 \text{ cm}^{-3}$, respectively.

combination of mass spectrometry and infrared laser Stark spectroscopy.

3.4. Predicted Gas-phase Abundance of CH₃O

As stated in Section 1, the reaction of OH with CH₃OH may have important implications for interstellar chemistry since it acts as a sink of methanol and a source of CH₃O radicals. In particular, here we are interested in evaluating whether or not this reaction can explain the observed abundance of CH₃O in the cold dense core B1-b, $\sim 5 \times 10^{-12}$ relative to H₂ or $\sim 3 \times 10^{-3}$ with respect to CH₃OH (Cernicharo et al. 2012).

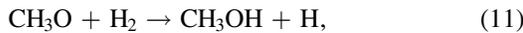
Figure 4 shows the time evolution of the predicted fractional abundances of the reactants involved in reaction (1), OH and CH₃OH, and the reaction product CH₃O for two different densities of H nuclei. It can be seen that methanol reaches its maximum abundance after a few 10^5 years (remember that the abundance of CH₃OH has been fixed to 6×10^{-5} relative to CO), while the methoxy radical increases its abundance progressively until reaching maximum at late times. The range of abundances of CH₃O relative to methanol, $n(\text{CH}_3\text{O})/n(\text{CH}_3\text{OH})$, achieved within a time range between 10^5 and 10^7 year is listed in Table 3. Our chemical model predicts that at $\sim 10^7$ year, $n(\text{CH}_3\text{O})/n(\text{CH}_3\text{OH})$ reaches a value of 2×10^{-3} or 0.6×10^{-3} , depending on the adopted density of H nuclei. This ratio is somewhat lower than, although of the same order as, that observed in B1-b. The main uncertainty in the calculated CH₃O/CH₃OH abundance ratio arises from the depletion rate of CH₃O, which in turn depends on the rate coefficients of the reactions of CH₃O with H and O atoms and on the abundances of H and O atoms, both species being very difficult to observe in cold, dense clouds. Nonetheless, with current constraints on the destruction rate of CH₃O, the title reaction is rapid enough at low temperatures to provide an efficient pure gas-phase pathway to CH₃O radicals in B1-b. Thus, our results indicate that the gas-phase formation of CH₃O via reaction (1), even though it does not fully interpret the observed abundance of methoxy radicals in B-1b, is likely to be a major contributor. Up to now, it has been thought that the main competing formation process of CH₃O is its synthesis on grain surfaces and further non-thermal desorption to the gas phase. As Cernicharo et al. (2012) pointed out, experiments that simulate ice-mantle processing by ultraviolet or ion irradiation indicate that it is not the CH₃O isomer, but the

Table 3
Calculated Abundances of CH₃O Relative to Methanol at 10 K Considering Gas-phase Formation Via Reaction (1)

Grain Surface Source of CH ₃ O	n_{H} (molecule cm ⁻³)	$k_1(10\text{ K})$ (cm ³ molecule ⁻¹ s ⁻¹)	$n(\text{CH}_3\text{O})/n(\text{CH}_3\text{OH})$	Time (year)	Reference
NO	2×10^4	1.1×10^{-10}	$(0.08-2) \times 10^{-3}$	10^5-10^7	This work
NO	1×10^5	1.1×10^{-10}	$(0.1-0.6) \times 10^{-3}$	10^5-10^7	This work
YES	2×10^4	3×10^{-10}	$\sim 5000 \times 10^{-3}$	10^5-10^7	Acharyya et al. (2015)
YES	1×10^5	4×10^{-11}	$(10-100) \times 10^{-3}$	10^5-10^7	Ruud et al. (2015)
NO	6×10^4	3×10^{-10}	$\sim 40 \times 10^{-3}$	$\sim 10^5$	Balucani et al. (2015)
NO	1×10^5	4×10^{-11}	$(2-10) \times 10^{-3}$	10^5-10^6	Vasyunin & Herbst (2013)
YES	1×10^5	4×10^{-11}	$(0.3-50) \times 10^{-3}$	10^5-10^6	Vasyunin & Herbst (2013)

Note. The observed $n(\text{CH}_3\text{O})/n(\text{CH}_3\text{OH})$ in B1-b is $\sim 3 \times 10^{-3}$ (Öberg et al. 2010; Cernicharo et al. 2012).

more stable isomer CH₂OH, which is formed on grain surfaces. This was proven by Chen et al. (2013), who observed CH₂OH in the X-ray irradiation of methanol ice at 14 K. The warming up of these ices produces ethylene glycol (CH₂OH)₂, indicating that the abundance of CH₂OH radicals is high. More recently, Lee et al. (2015) observed that CH₃O formed in the 355 nm irradiation of a *p*-H₂ matrix containing methyl nitrite (CH₃ONO) at 3.2 K is rapidly converted into CH₂OH. These authors theoretically predict that the conversion of CH₃O to CH₂OH on grain surfaces may occur in two steps:



In light of these results, the formation of CH₃O through grain-surface processes seems to be disfavored, although more laboratory experiments and/or quantum chemistry calculations are needed to draw definitive conclusions.

3.4.1. Comparison with Previous Chemical Models

In Table 3, some input parameters used in previous chemical models and the predicted abundances of CH₃O are listed for comparison purposes. The first column of the table indicates whether or not the model includes grain-surface production of CH₃O radicals and the second column provides the density of H nuclei adopted in each model. As can be seen in the third column, the rate coefficient $k_1(10\text{ K})$ used in previous models, either 4×10^{-11} cm³ molecule⁻¹ s⁻¹ (measured by Shannon et al. 2013 at 63 K) or 3×10^{-10} cm³ molecule⁻¹ s⁻¹ (collision limit), differs by almost one order of magnitude. The fourth column gives the range of CH₃O/CH₃OH abundance ratios predicted by each model over a certain time interval, indicated in the fifth column.

Our results are consistent with those of Vasyunin & Herbst (2013) when grain-surface production of CH₃O is switched off in their model and reaction (1) becomes the only efficient formation route to CH₃O. The CH₃O/CH₃OH abundance ratios reported by Vasyunin & Herbst (2013) are around or slightly above 10^{-3} , while ours are around or slightly below 10^{-3} . Balucani et al. (2015) only consider gas-phase formation of CH₃O with $k_1(10\text{ K}) = 3 \times 10^{-10}$ cm³ molecule⁻¹ s⁻¹ and find a CH₃O/CH₃OH abundance ratio of $\sim 4 \times 10^{-2}$, which is about 10 times higher than the value observed in B1-b, over a restricted time interval of around 10^5 year.

As seen in Table 3, a common outcome of models that consider formation of CH₃O on grain surfaces (Vasyunin & Herbst 2013; Acharyya et al. 2015; Ruud et al. 2015) is a significant overestimation of the CH₃O/CH₃OH abundance ratio with respect to the observed value in B1-b. This fact

points to an overestimate for the formation efficiency of CH₃O through grain-surface routes, which is consistent with the empirical conclusion that CH₃O is not predominantly formed on grains surfaces. It must be noted that the efficiency of the grain-surface processes invoked to explain the formation of CH₃O is highly uncertain.

In the chemical models of Vasyunin & Herbst (2013) and Ruud et al. (2015), CH₃O is assumed to be formed mainly on the surface of dust grains through successive hydrogenations of CO. Methoxy radicals are assumed to be further ejected to the gas phase through chemical desorption, which assumes that a fraction, typically 1%, of the energy released by exothermic chemical reactions on grain surfaces is used by the products to desorb. In the chemical model of Ruud et al. (2015), CH₃O is also formed through a mechanism involving the formation of van der Waals complexes between carbon atoms colliding with dust grains and water-ice molecules. In these two chemical models, the formation of CH₃O through the gas-phase reaction of OH and CH₃OH was included, although grain-surface processes are found to dominate the formation of CH₃O. The gas-phase production rate of CH₃O is similar in both models, although the depletion of CH₃O through reactions with H and O atoms is assumed to be faster in the model of Vasyunin & Herbst (2013). This means that, as seen in Table 3, the values of $n(\text{CH}_3\text{O})/n(\text{CH}_3\text{OH})$ predicted by Ruud et al. (2015) are higher than those calculated by Vasyunin & Herbst (2013).

Acharyya et al. (2015) modeled the fractional abundance of CH₃O using an updated gas-grain chemical model that included the gas-phase reaction of OH with methanol (reaction (1)) and with some other organic molecules. These authors run the model with and without reaction (1) and concluded that at 10 K this reaction is not generally an effective destruction route for CH₃OH, although it leads to an increase in the abundance of CH₃O at times longer than 2×10^5 year. The main competing process for the formation of gas-phase CH₃O in this model is the hydrogenation of formaldehyde on grain surfaces followed by non-thermal desorption. Clearly, in this model, the CH₃O/CH₃OH abundance ratio is largely overestimated with respect to the observed value in B1-b, probably as a consequence of the too efficient formation of CH₃O via grain-surface routes.

4. CONCLUSIONS

In this work, we have determined the rate coefficient k_1 for the gas-phase reaction between OH radicals and CH₃OH in the range of temperatures between 22 and 64 K. This study provides the first measurement of k_1 at temperatures below 56 K. The lowest temperature investigated here, 22 K, is the closest one to that in B1-b for which the rate coefficient of the

reaction between OH and CH₃OH has been measured. In the cold environment of B1-b, CH₃O (product of the reaction between OH and CH₃OH) has recently been detected. The consistency of the measured rate coefficients in two different laboratories (UCLM and UR1) gives us confidence in the reported $k_1(T)$, especially around 60 K where there is some discrepancy with previous data. We fit the measured rate coefficients as a function of temperature and provide an expression of $k_1(T)$ in the temperature range 22–64 K. Further measurements of k_1 at temperatures below 22 K are needed to corroborate whether or not this reaction continues to be accelerated at even lower temperatures and to constrain by how much in order to better evaluate its contribution to the production of CH₃O in cold, dense clouds such as B1-b. In addition, there is still a gap to fill between 64 and 123 K, which will be covered in the near future using new Laval nozzles that will help to elucidate the kinetic behavior at intermediate temperatures. Finally, we will intend to detect CH₃O radicals formed in the reaction of OH with methanol at 22 K by LIF. This is planned for the near future, since some changes are needed in the experimental system to detect CH₃O.

We have also modeled the chemistry of CH₃O in cold, dense clouds considering that it is only formed through the gas-phase reaction of OH and CH₃OH. We have adopted the extrapolated value of $k_1(T)$ at 10 K and assumed that gas-phase reactions with H and O atoms are the only removal processes of CH₃O. This model predicts CH₃O/CH₃OH abundance ratios that are similar or slightly below the value observed in B1-b ($\sim 3 \times 10^{-3}$), confirming that the reaction of OH and CH₃OH is clearly involved in the formation of interstellar methoxy radicals. This is consistent with recent experiments that indicate that CH₂OH, rather than CH₃O, is the isomer formed on icy grain mantles. Nonetheless, the role of grain-surface processes on the chemistry of CH₃O needs to be further investigated. A search for the more stable isomer, CH₂OH, in cold dense clouds may shed light on the relative role of gas-phase and grain-surface chemical reactions in the synthesis of methanol-derived radicals. To date, the rotational spectrum of CH₂OH has not yet been accurately measured in the laboratory, which complicates detection in the interstellar medium.

This work has been supported by the European Research Council and the Spanish Ministry of Science and Innovation through the NANOCOSMOS (SyG-610256) and ASTROMOL (CSD2009-00038) projects, respectively. Authors from UCLM and CSIC acknowledge the Spanish Ministry of Economy and Competitiveness for supporting this work under projects GASSOL (CGL2013-43227-R), AYA2009-07304, and AYA2012-32032. Authors from UR1 thank the French national programme PCMI “Physique et Chimie du Milieu

Interstellaire” from INSU (Institut National des Sciences de l’Univers) for financial support. A.C. is grateful to UCLM for providing him with an invited researcher position for 5 months. Authors thank GM Muñoz Caro for helpful discussions.

REFERENCES

- Acharyya, K., Herbst, E., Caravan, R. L., et al. 2015, *MolPh*, **113**, 2243
 Agúndez, M., & Wakelam, V. 2013, *ChRv*, **113**, 8710
 Atkinson, R., Baulch, D. L., Cox, R. A., et al. 2006, *ACP*, **6**, 3625
 Balucani, N., Ceccarelli, C., & Taquet, V. 2015, *MNRAS*, **449**, L16
 Baulch, D. L., Bowman, C. T., Cobos, C. J., et al. 2005, *JPCRD*, **34**, 757
 Canosa, A., Goulay, F., Sims, I. R., & Rowe, B. R. 2008, in *Low Temperatures and Cold Molecules*, ed. I. W. M. Smith (London: Imperial College Press), 55
 Caravan, R. L., Shannon, R. J., Lewis, T., et al. 2015, *JPCA*, **119**, 7130
 Cernicharo, J., Marcelino, N., Roueff, E., et al. 2012, *ApJL*, **759**, L43
 Chen, Y.-J., Ciaravella, A., Muñoz Caro, G. M., et al. 2013, *ApJ*, **778**, 162
 Cheng, B.-M., Bahou, M., Cheng, W.-C., et al. 2002, *JChPh*, **117**, 1633
 Daniel, F., Gerin, M., Roueff, E., et al. 2013, *A&A*, **560**, A3
 Dóbé, S., Bérces, T., & Szilágyi, I. 1991, *J. Chem. Soc. Faraday Trans.*, **87**, 2331
 El Dib, G., Sleiman, C., Canosa, A., et al. 2013, *JPCA*, **117**, 117
 Ewig, F., Rhasa, D., & Zellner, R. 1987, *Ber. Bunsen. Phys. Chem.*, **91**, 708
 Gómez Martín, J. C., Caravan, R. L., Blitz, M. A., et al. 2014, *JPCA*, **118**, 2693
 Herbst, E., & Leung, C. M. 1989, *ApJS*, **69**, 271
 Hernandez, F. J., Brice, J. T., Leavitt, C. M., et al. 2015, *JPCA*, **119**, 8125
 Hoyermann, K., Sievert, R., & Wagner, H. G. 1981, *Ber. Bunsen. Phys. Chem.*, **85**, 149
 Jiménez, E., Antiñolo, M., Ballesteros, B., et al. 2016, *PCCP*, **18**, 2183
 Jiménez, E., Ballesteros, B., Canosa, A., et al. 2015, *RSci*, **86**, 045108
 Jodkowski, J. T., Rayez, M.-T., & Rayez, J.-C. 1999, *JPCA*, **103**, 3750
 Kalváns, J. 2015, *ApJ*, **806**, 196
 Laksmo, H., Tanimura, S., Allen, H. C., et al. 2011, *PCCP*, **13**, 5855
 Lee, Y.-P., Chou, W.-T., Johnson, B. A., et al. 2015, *JMoSp*, **310**, 57
 Li, D., & Goldsmith, P. F. 2003, *ApJ*, **585**, 823
 Lis, D. C., Roueff, E., Gerin, M., et al. 2002, *ApJL*, **571**, L55
 McElroy, D., Walsh, C., Markwick, A. J., et al. 2013, *A&A*, **550**, 36
 Öberg, K. I., Bottinelli, S., Jørgensen, J. K., & van Dishoeck, E. F. 2010, *ApJ*, **716**, 825
 Reboussin, L., Wakelam, V., Guilloteau, S., & Hersant, F. 2014, *MNRAS*, **440**, 3557
 Ruaud, M., Loison, J.-C., Hickson, K. M., et al. 2015, *MNRAS*, **447**, 4004
 Sanders, N., Butler, J. E., Pasternack, L. R., & McDonald, J. R. 1980, *CP*, **49**, 17
 Shannon, R. J., Blitz, M. A., Goddard, A., & Heard, D. E. 2013, *NatCh*, **5**, 745
 Shannon, R. J., Caravan, R. L., Blitz, M. A., & Heard, D. E. 2014, *PCCP*, **16**, 3466
 Shannon, R. J., Taylor, S., Goddard, A., et al. 2010, *PCCP*, **12**, 13511
 Sims, I. R. 2013, *NatCh*, **5**, 734
 Sims, I. R., Queffelec, J.-L., Defrance, A., et al. 1994, *JChPh*, **100**, 4229
 Smith, I. W. M., & Barnes, P. W. 2013, *Annu. Rep. Prog. Chem. C*, **109**, 140
 Smith, I. W. M., Herbst, E., & Chang, Q. 2004, *MNRAS*, **350**, 323
 Vasyunin, A. I., & Herbst, E. 2013, *ApJ*, **769**, 34
 Vöhringer-Martínez, E., Hansmann, B., Hernández, H., et al. 2007, *Sci*, **315**, 497
 Wakelam, V., Loison, J.-C., Herbst, E., et al. 2015, *ApJS*, **217**, 20
 Wang, B., Hou, H., & Gu, Y. 1999, *JPCA*, **103**, 8021